Power Research - A Journal of CPRI, Vol 22(1), 2026 | pp. 105-118

Failure Forensics of a 31.5 MVA Power Transformer: Cumulative Through-Fault Aging Leading to a Catastrophic Arcing Interturn Fault

B. Venu Madhav[1], H. Ganganna[2] and R. S. Chanakya Vardhan Reddy[3]*

[1]EE/MRT & TRs/Kurnool, Transmission Corporation of Andhra Pradesh Limited (APTRANSCO), Kurnool - 518001, Andhra Pradesh, India

[2]DEE/TRE/Kurnool, Transmission Corporation of Andhra Pradesh Limited (APTRANSCO), Kurnool - 518001, Andhra Pradesh, India

[3]AEE/MRT/Nandyal, Transmission Corporation of Andhra Pradesh Limited (APTRANSCO), Nandyal - 518501, Andhra Pradesh, India; rscvreddy@gmail.com

Keywords: Differential Protection, Dissolved Gas Analysis, Excitation Current, Internal Inspection, Interturn Fault, Polarization Index (PI), Power Transformer, SFRA

Article Received: 22-06-2026
Article Revised: 23-07-2026
Article Accepted: 28-09-2026

DOI: 10.33686/pwj.22.1.2026.105-118

*Author for correspondence

Abstract

A 31.5 MVA, 220/11 kV TELK power transformer failed during energization after approximately 17 years of service. The failure-event COMTRADE record captured assertion of the main-tank pressure-relief-device (PRV) input at 488.475 ms, followed by the 86 internal-trip and PRV-annunciation channels at 490.980 ms, while differential annunciation and the three phase-trip bits remained deasserted. The installed GE MiCOM P643 used 100/1 A HV CTs, 2000/0.5775 A LV CTs (approximately 3464/1), and an Is1 pickup of 0.2 pu. Post-failure DGA measured 56.29 ppm acetylene and 111.18 ppm ethylene; Duval, Rogers, industry three-ratio, and an APTRANSCO-developed machine-learning ensemble classified the discharge as D2, with the ensemble assigning 87% probability. The LV R-phase resistance was 19.91% above the Y/B mean, its turns-ratio error remained 1.54–2.64% over all 17 tap positions, and its excitation current was 9.30 times the Y/B mean. In SFRA, the large low-frequency R-phase separation appeared with the LV winding electrically open and collapsed when the LV was shorted, identifying the reduced-turn/magnetizing-inductance signature of an LV R-phase interturn short. The convergent chemical, electrical, dielectric, frequency-response, protection, and physical evidence establishes a high-energy arcing interturn fault. The recorded operating history — repeated LV-side faults from reptile intrusion and cable puncture — and the measured winding deformation establish cumulative through-fault electrodynamic aging as the failure pathway. The principal contributions are a cross-validated multi-physics forensic workflow and an APTRANSCO-developed machine-learning DGA ensemble that independently corroborates the classical D2 diagnosis, applied here to establish cumulative through-fault aging — rather than a single triggering event — as the operative failure mechanism.

This is an open access article under the terms of the CC BY: Allows others to copy, distribute, and build upon the work for any purpose, provided they credit the original creator

© 2026 The Author(s). *Central Power Research Institute* published by Informatics Publishing Limited

1. INTRODUCTION

Power transformers are indispensable assets in electrical transmission and distribution networks, and their operational reliability is paramount to grid stability. An unexpected failure of a high-voltage transformer can lead to significant service interruptions, substantial economic losses from repair or replacement, and potential collateral damage. Consequently, the accurate diagnosis of faults and an understanding of their underlying progression mechanisms are cornerstones of modern condition-based asset management strategies. The longevity and reliability of these critical assets are primarily dictated by the health of their insulation systems, which are subject to irreversible degradation over their operational life.

Among the most challenging and insidious failure modes are winding interturn faults, which are one of the most frequent faults experienced by power transformers. These faults often begin as minor, incipient insulation degradation between adjacent conductors, a slow process driven by the cumulative effects of thermal, electrical, and chemical stresses. Over time, this degradation can progress from partial discharges to a low-impedance short circuit. A critical characteristic of these faults, particularly in their early stages, is that they produce a very small change in the transformer's terminal currents. This phenomenon, often described as the "autotransformer effect," occurs because the full winding acts as the primary of an autotransformer, while the few shorted turns act as a heavily loaded secondary. While the circulating current within the shorted loop itself can be extremely high, the reflected change in the total line current is stepped down by the high turns ratio between the full winding and the faulted section. As a result, the resulting differential current often falls below the sensitivity threshold of standard differential protection relays, rendering them unable to detect the fault until it escalates into a more severe event, such as a phase-to-ground or phase-to-phase fault. By that point, significant and often irreparable damage to the winding and core has already occurred.

This behaviour is an important limitation of protection philosophies that depend primarily on terminal current. It also explains the diagnostic value of mechanical protection and condition measurements. Cellulose insulation loses mechanical and dielectric strength under thermal, moisture, and oxidation stress, while external short circuits impose high electrodynamic forces on winding conductors and clamping structures[1,2]. In this case, the operating register establishes recurrent through-fault exposure, and the pre-event insulation-resistance values and tan-delta/capacitance trend establish the condition history. The phase-selective electrical tests, low-frequency SFRA response, and physical deformation then identify the accumulated consequence in the LV R-phase winding.

This paper reconstructs the failure by correlating PRV operation and COMTRADE data with DGA, winding tests, dielectric trends, three SFRA configurations, relay settings, and internal inspection. The objectives are to localize the fault, evaluate the installed protection response, and test the proposed cumulative through-fault mechanism against the measured evidence.

2. CASE STUDY: SYSTEM PARAMETERS AND FAILURE CHRONOLOGY

2.1 Asset Specification

Table 1. Specifications of transformer

Parameter	Details
Manufacturer	TELK
Voltage rating	220/11 kV
Power rating	31.5 MVA
Vector group	YNyn0
Year of manufacture	2008
Cooling class	ONAN/ONAF
OLTC	TELK make, D2 type; IEC 60214-1 [3]
Transformer differential relay	GE MiCOM P643
Differential CT ratios	HV 100/1 A; LV 2000/0.5775 A (approximately 3464/1)

2.2 The Failure Event

During the energization associated with the failure, the COMTRADE record captured a 488 ms interval from record start to trigger, and the main-tank PRV input (L6) asserted at 488.475 ms. The record does not contain a breaker-close transition; therefore, the 488 ms value is retained only on the relay-record time base and is not interpreted as arc duration or PRV operating time.

2.3 Protection Response

Transformer differential protection was provided by a GE MiCOM P643 [4] relay with 100/1 A HV CTs and 2000/0.5775 A LV CTs (approximately 3464/1). The installed settings were Is1 = 0.2 pu, K1 = 20%, Is2 = 5.0 pu, and K2 = 60%; Idiff high-set = 12 pu, transient bias, second-harmonic blocking at 15%, cross-blocking, CT-saturation detection, and zero-sequence filtering on both windings were enabled. In the failure-event record, the PRV input asserted before the 86 internal-trip, spare-output, and PRV-annunciation channels, which changed at 490.980 ms. Differential annunciation and Idiff trip A/B/C remained deasserted. The installed settings and the complete analog/digital sequence are presented in Figure 11 (Section 4.3).

3. COMPREHENSIVE POST-FAULT DIAGNOSTIC INVESTIGATION

Following the failure, a comprehensive diagnostic investigation determined the fault type and location by correlating chemical analysis of the insulating oil with electrical, dielectric, frequency-response, protection, and internal-inspection evidence. The independent observations converge on one diagnosis and one phase location.

3.1 Chemical Analysis: Dissolved Gas Analysis (DGA)

The post-failure oil sample was analyzed by DGA, and Table 2 gives the measured concentrations. Interpretation follows IEC 60599 and IEEE C57.104 [5,6], with sampling and analytical practice referenced to IEC 60567 and IEC 60475 [7,8]. The multi-method computational workflow combines Duval geometry, ratio methods, and an APTRANSCO-developed machine-learning ensemble[9].

Table 2. Dissolved gas analysis results

Gas	Measured Value (ppm)
Hydrogen	24.70
Methane	21.79
Ethane	17.69
Ethylene	111.18
Acetylene	56.29
Carbon Monoxide	53.42
Carbon Dioxide	791.20

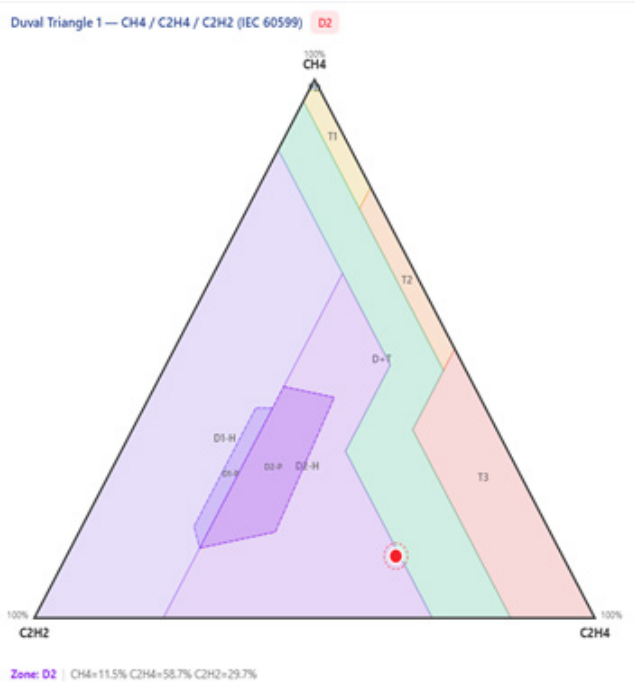


Figure 1. Duval Triangle-1 result from the post-fault DGA concentrations; the point is located in the D2 high-energy discharge region.

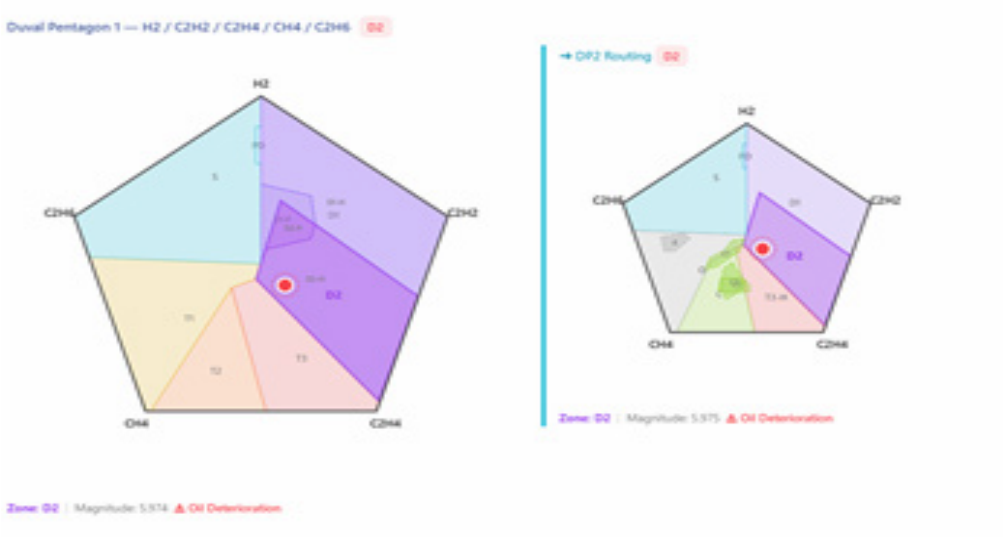


Figure 2. Duval Pentagon-1/2 results from the post-fault DGA concentrations; both plots indicate the D2 region.

The post-fault gas profile contained 56.29 ppm acetylene (C_2H_2) and 111.18 ppm ethylene (C_2H_4). The total dissolved combustible gas concentration, excluding CO_2, was 285.07 ppm. The calculated hydrocarbon percentages for Duval Triangle-1 were CH_4 = 11.5%, C_2H_4 = 58.7%, and C_2H_2 = 29.7%. The plotted point lies securely in the D2 region and establishes a high-energy electrical-discharge signature[5,6].

The D2 gas signature and the recorded main-tank PRV input are two measurements of the same internal arcing sequence: the interturn arc decomposed the surrounding oil, generated combustible gas and produced the pressure rise that operated the mechanical protection. COMTRADE timing, DGA chemistry, and internal carbonization therefore form a continuous causal chain.

The ratios C_2H_2/C_2H_4 = 0.506, CH_4/H_2 = 0.882, and C_2H_4/C_2H_6 = 6.286 provide an independent cross-check. Rogers three-ratio and the industry Ra/Rb/Rc method both classify the pattern as D2; the IEC 60599 table directs correlation for this ratio combination, and the key-gas method identifies arcing (Figure 3). As a data-driven cross-check, an APTRANSCO-developed soft-voting ensemble combining XGBoost, LightGBM-

Independent DGA ratio and key-gas classifications

Method	Measured diagnostic quantities	Result
Rogers three-ratio	C2H2/C2H4 = 0.506; CH4/H2 = 0.882 C2H4/C2H6 = 6.286	D2
IEC 60599 ratio table	Measured ratio combination lies outside a single-code row	Correlate
Industry three-ratio	Ra = 1.591; Rb = 0.702; Rc = 0.506	D2
IEEE C57.104 key-gas check	C2H2 = 56.29 ppm; C2H4 = 111.18 ppm	Arcing

Multi-method consensus: D2 high-energy electrical discharge

Figure 3. Independent ratio and key-gas cross-check. Rogers and the industry three-ratio method classify D2, while the combined multi-method result identifies high-energy arcing.



Figure 4. APTRANSCO-developed soft-voting DGA ensemble trained and validated on the IEC TC10 labelled dataset. XGBoost, LightGBM-DART, and random forest all classify the case as D2; the ensemble assigns 87% probability, with 90.3% validation accuracy and 89.4% macro-F1.

DART, and random forest was trained and validated on the labelled IEC TC10 DGA dataset[10]. It achieved 90.3% validation accuracy and 89.4% macro-F1; all three base learners classified this case as D2, and the ensemble assigned D2 an 87% probability (Figure 4). Duval geometry, ratio methods, and key-gas analysis together establish the D2 high-energy-discharge diagnosis; the independently trained ensemble corroborates this classification and is, in turn, validated by its agreement with the established methods[5,6,9,10].

3.2 Electrical Integrity Assessment of Windings

Post-event electrical tests localized and characterized the winding anomaly. Table 3 summarizes the phase measurements and their quantitative comparison. Resistance, ratio, and excitation results provide three mutually reinforcing measurements of the same LV R-phase interturn fault[11,12].

3.2.1 Winding Resistance

The LV R-phase resistance was 5.069 mΩ, compared with 4.192 mΩ and 4.263 mΩ for the Y and B phases. Relative to the Y/B mean of 4.2275 mΩ, the R-phase value was 19.91% higher, while the Y-B spread was only 1.68% of their mean; the measurements were obtained at 42 °C. This large phase-selective rise establishes an arc-damaged R-phase conductor path with reduced effective current-carrying section, consistent with the recovered copper particles and carbonization[11].

Table 3. Synthesis of LV winding electrical test results

Test	R phase	Y phase	B phase	Interpretation
Resistance	5.069 mΩ	4.192 mΩ	4.263 mΩ	Arc-damaged R-phase path
Ratio error, tap 5	+2.19%	+0.33%	+0.28%	Reduced turns; interturn short
Excitation current	4.0 A	0.41 A	0.45 A	Shorted-turn loop; R = 9.30 × Y/B mean

3.2.2 Turns Ratio

The turns-ratio test used approximately 245–250 V on the HV side and covered all 17 taps. The R-phase error remained positive at every tap, ranging from +1.54% to +2.64%, with a maximum of +2.64% at tap 1. At tap 5, the errors were +2.19% (R), +0.33% (Y), and +0.28% (B); at tap 9 they were +2.02%, +0.12%, and +0.12%, respectively. The persistence across the complete tap range excludes an isolated tap-contact effect and establishes a reduced-effective-turn condition in the LV R-phase, the expected ratio signature of shorted turns. Interpreted as a first-order estimate, this deviation implies that approximately 2% of the LV R-phase turns (about 2.0–2.6%) were short-circuited, since the fractional turn reduction is approximately equal to the per-unit ratio error for a small shorted section; this few-turn condition is consistent with the autotransformer effect that keeps the reflected differential current small. Figure 5 presents the complete measured trend[11].

3.2.3 Excitation Current

In the single-phase excitation-current test, the HV winding was open and comparable voltages of 246.1 V, 248.0 V, and 247.6 V were applied to the LV R, Y, and B phases, respectively. The measured currents were 4.0 A, 0.41 A, and 0.45 A. The R-phase current was 9.30 times the Y/B mean; the applied-voltage spread was less than 1%, so voltage variation cannot account for the response. This ninefold phase-selective increase establishes a low-impedance circulating turn loop that reduced the effective magnetizing inductance of the LV R-phase[11].

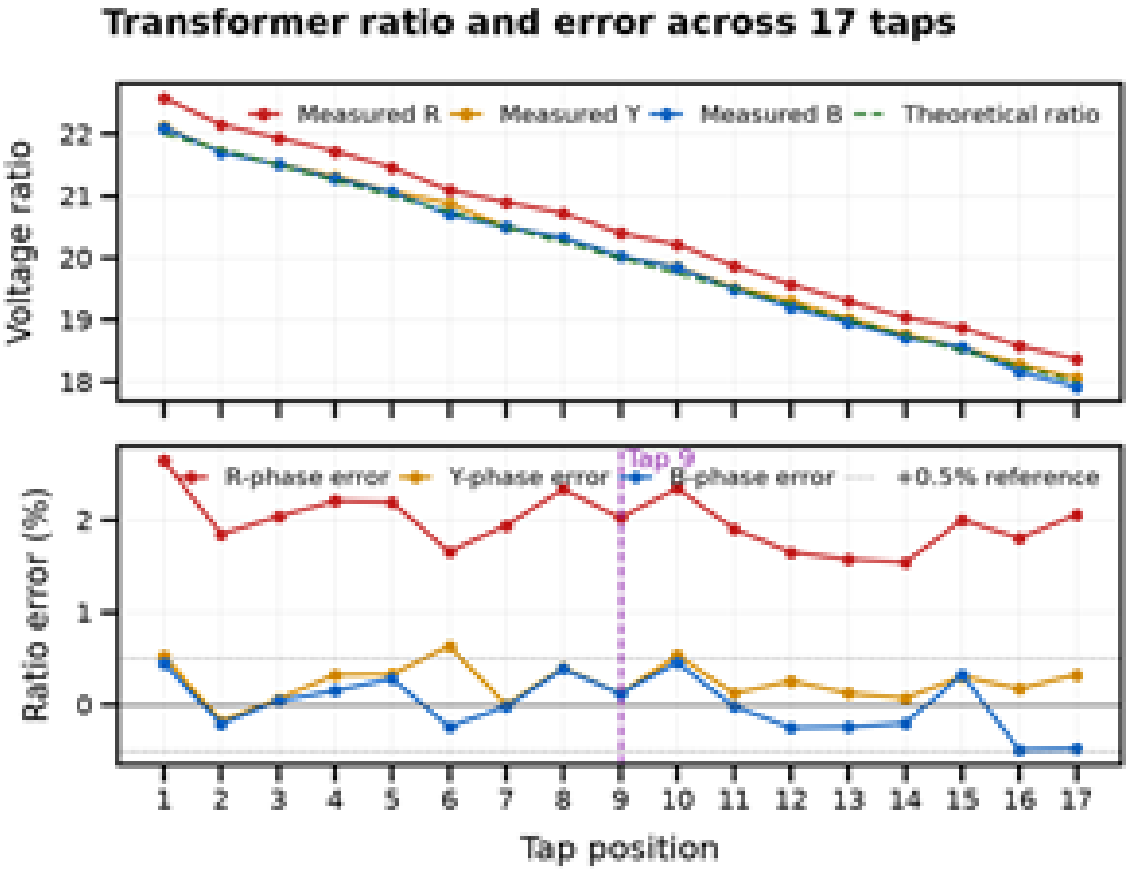


Figure 5. Measured transformer ratio and percentage error for the R, Y, and B phases over all 17 tap positions.

The simultaneous 19.91% resistance increase, persistent positive ratio error, and 9.30-fold excitation-current rise form a diagnostic triad: the R-phase conductor path was arc-damaged, effective turns were reduced, and a shorted-turn circulating loop was present. Internal carbon deposits, copper particles, and damaged paper insulation physically confirm this electrical diagnosis.

3.3 Insulation System Condition Assessment

The insulation-resistance, PI, tan-delta, and capacitance results were arranged as a condition sequence comprising two pre-event baselines and one post-event measurement. This sequence separates the historical bulk-insulation condition from the dielectric changes observed after arcing.

At 5 kV, the post-event PI values were 1.30 for HV-LV, 1.42 for HV-body, and 0.80 for LV-body. The LV-body insulation resistance decreased from 75 MΩ at 60 s to 60 MΩ at 600 s. The sub-unity PI and falling resistance establish a conductive LV-to-ground insulation path created by carbonized oil-paper residue after the arc[12].

At the measured test condition, the winding dissipation factors at 5 kV were 0.284% for HV-LV, 0.106% for HV-body, and 0.713% for LV-body; the corresponding capacitances were 3788 pF, 6205 pF, and 12120 pF. Figure 6 gives the values corrected to 20 °C. The post-event LV-body point rises to approximately 0.44%, compared with approximately 0.12–0.16% at the two baselines, while LV-body capacitance falls from approximately 17 nF to 12.1 nF. This simultaneous increase in dielectric loss and decrease in capacitance establishes deterioration of the LV-to-ground oil-paper path at the faulted winding. The loss increase reflects the conductive carbonized residue at the fault site, and the capacitance reduction is consistent with the documented LV R-phase winding deformation.

A representative pre-failure megger check recorded 2.53 GΩ for HV-body, 4.42 GΩ for LV-body, and 5.89 GΩ for HV-LV. These high bulk-insulation values

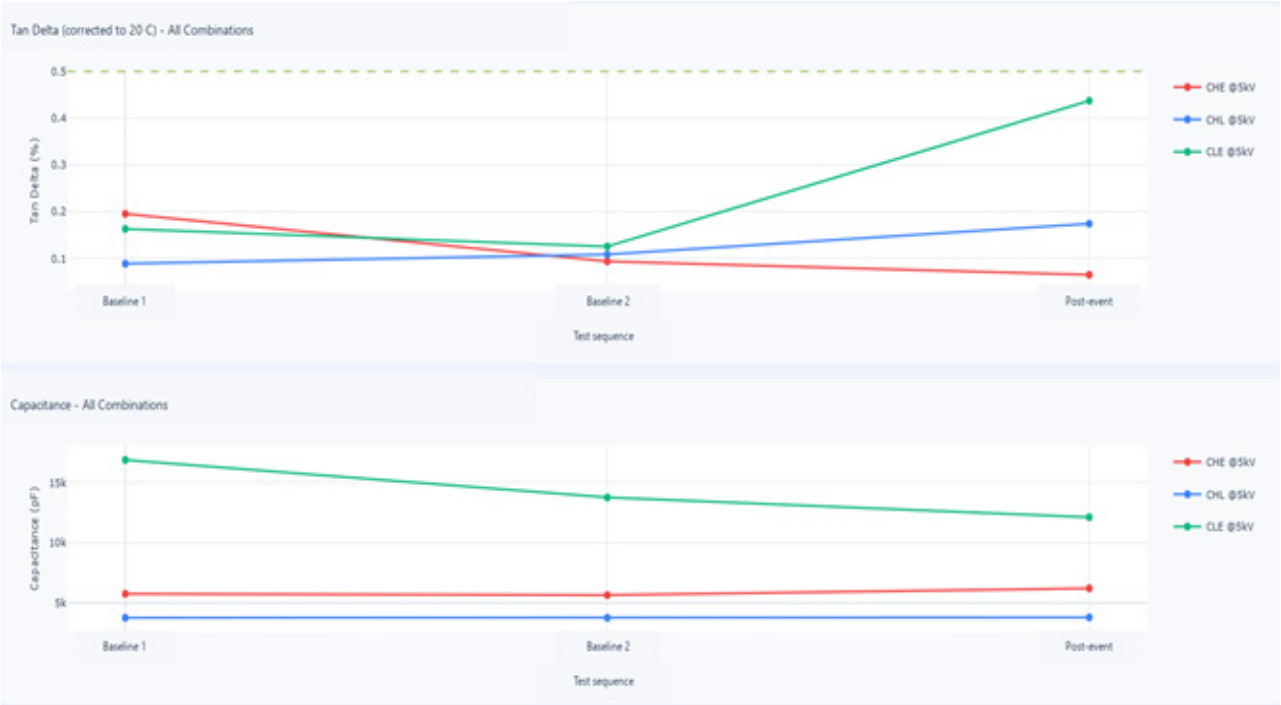


Figure 6. Anonymized tan-delta (corrected to 20 °C) and capacitance comparison across two baselines and the post-event measurement.

show that the defect was localized between turns rather than distributed through the complete winding-to-ground insulation. After the failure, the low LV-body PI/IR and the tan-delta/capacitance shift directly track the carbonaceous contamination and damaged oil-paper insulation documented during internal inspection.

3.4 Structural Integrity Assessment: Sweep Frequency Response Analysis (SFRA)

SFRA was acquired with a Megger FRAX system over 20 Hz to 2 MHz in three complementary configurations: LV response with the HV winding open; HV response with the LV winding open; and HV response with the LV winding shorted. Phase-to-phase comparison is decisive in this three-phase unit because the healthy Y and B traces provide two simultaneous in-service references, while the open/short configuration change separates the LV magnetizing-turn contribution from the HV response. Correlation Coefficient (CC) and RMS magnitude difference are reported through 1 MHz in accordance with IEC 60076-18 and IEEE C57.149 [13,14].

The complete LV response with the HV winding open is presented in Figure 7. In the 20 Hz–2 kHz core/turns band, CC/RMS values were 0.522/8.59 dB for R-Y and 0.609/7.51 dB for R-B, compared with 0.989/1.28 dB for Y-B. The two healthy phases remain essentially coincident while the R-phase separates strongly. This is the low-frequency signature of reduced effective turns and magnetizing inductance produced by an LV R-phase interturn short.

Figure 8 adds the two HV-response configurations. With the LV winding open, the 20 Hz–2 kHz R-Y and

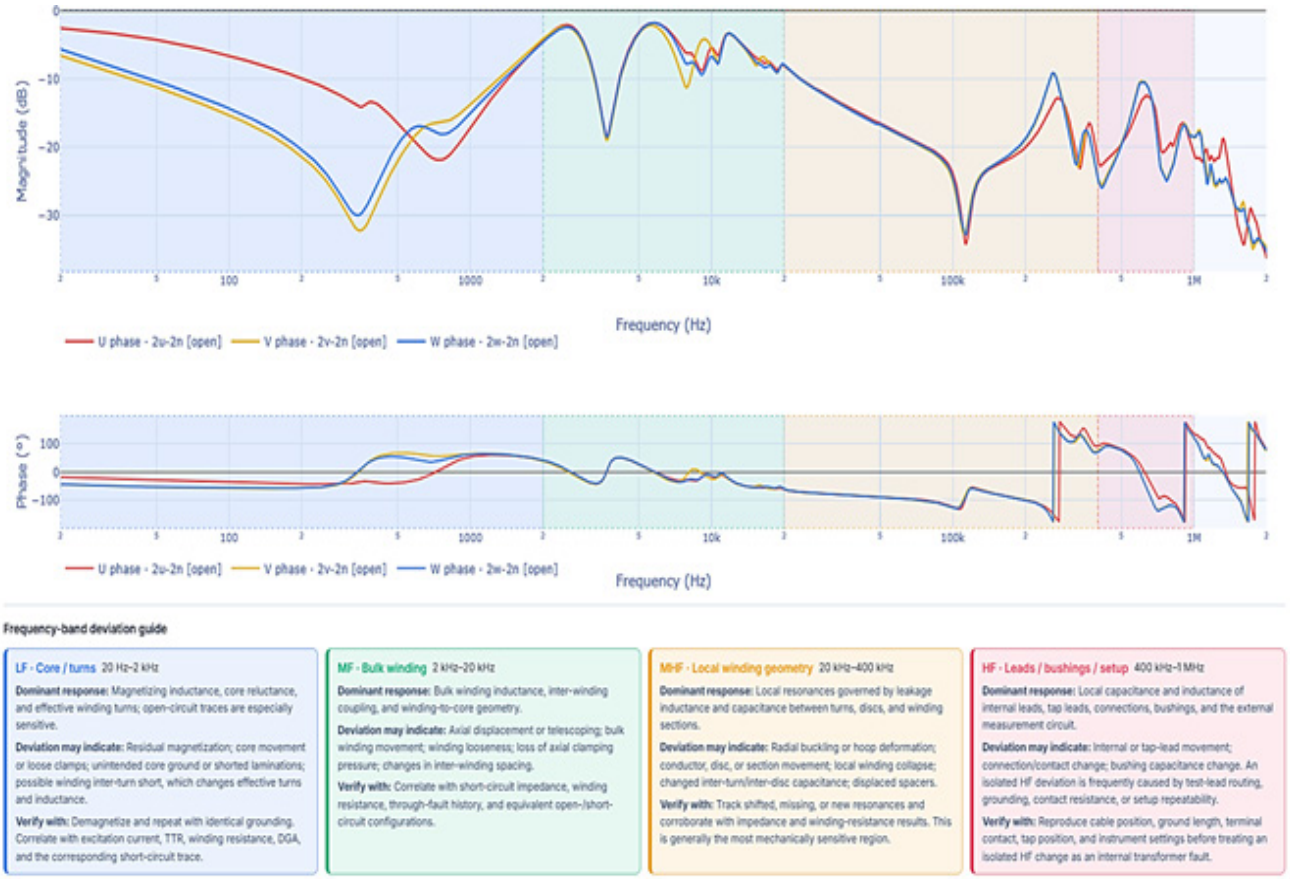


Figure 7. Complete LV response with the HV winding open, showing the decisive low-frequency R-phase separation in magnitude and phase together with the frequency-band interpretation guide.

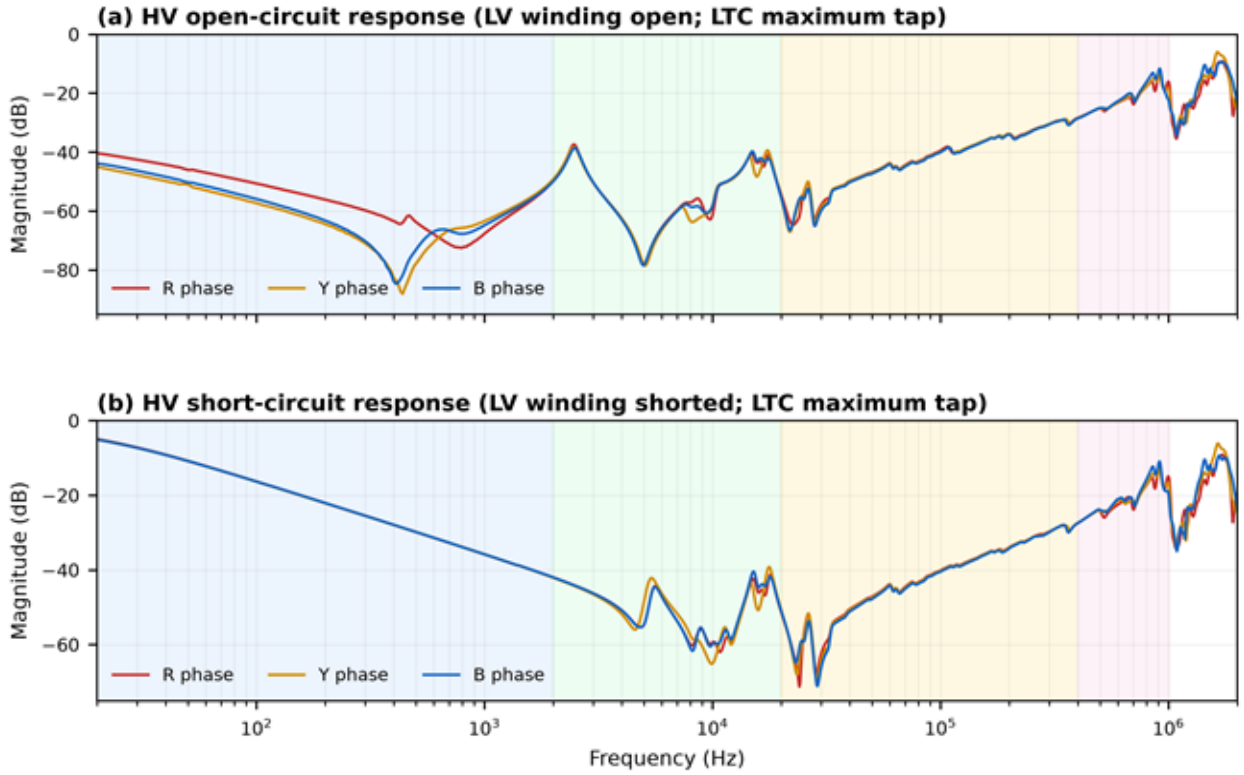


Figure 8. Companion SFRA configurations: **(a)** HV response with the LV winding open and **(b)** HV response with the LV winding shorted. The low-frequency R-phase separation disappears when the LV is shorted, localizing the interturn defect to the LV winding.

Cell format: correlation coefficient (CC) / RMS magnitude difference (dB)

Configuration	Pair	20 Hz-2 kHz	2-20 kHz	20-400 kHz	400 kHz-1 MHz
LV response HV open	R-Y	0.5224 / 8.59	0.9291 / 1.48	0.9733 / 1.23	0.9357 / 2.23
	R-B	0.6092 / 7.51	0.9942 / 0.55	0.9706 / 1.29	0.9386 / 2.34
	Y-B	0.9894 / 1.28	0.9358 / 1.34	0.9979 / 0.35	0.9998 / 0.24
HV response LV open	R-Y	0.7877 / 8.21	0.9822 / 2.04	0.9957 / 0.89	0.9771 / 0.89
	R-B	0.8410 / 6.91	0.9961 / 0.93	0.9941 / 1.13	0.9559 / 1.55
	Y-B	0.9870 / 1.86	0.9866 / 1.74	0.9987 / 0.60	0.9832 / 1.03
HV response LV short	R-Y	1.0000 / 0.07	0.9234 / 2.42	0.9972 / 0.81	0.9727 / 0.94
	R-B	1.0000 / 0.05	0.9912 / 0.81	0.9926 / 1.35	0.9612 / 1.40
	Y-B	1.0000 / 0.06	0.9178 / 2.51	0.9978 / 0.76	0.9848 / 0.94

Figure 9. Phase-pair CC and RMS magnitude difference for all three SFRA configurations and four frequency bands; the low-frequency metrics quantify the LV R-phase interturn signature.

R-B comparisons were 0.788/8.21 dB and 0.841/6.91 dB, whereas Y-B was 0.987/1.86 dB. When the LV winding was shorted, all three low-frequency phase pairs became coincident: CC exceeded 0.99999 and RMS difference remained below 0.08 dB. Shorting the LV suppresses its magnetizing-turn contribution; the disappearance of the R-phase separation therefore demonstrates that the low-frequency defect originates in the LV winding, not the HV winding or core.

Figure 9 reports CC/RMS values for every phase pair, configuration, and frequency band. The decisive 20 Hz–2 kHz separation identifies the interturn/effective-turn defect, while the R-phase differences through the medium- and high-frequency bands identify the accompanying local winding-geometry and lead-region disturbance. In the complete LV response, R-Y and R-B RMS differences at 400 kHz–1 MHz were 2.23 dB and 2.34 dB, compared with only 0.24 dB for Y-B. The same R-phase selectivity appears in the HV response only while the LV remains open, completing the electrical localization[14,15].

The complete LV waveform, the two companion HV responses, and the all-configuration CC/RMS matrix establish an LV R-phase interturn fault. The low-frequency R-phase separation is large with the LV electrically active and collapses under LV short circuit, exactly as expected when shorted turns reduce effective turns and magnetizing inductance. Agreement with the persistent TTR offset, ninefold excitation current, elevated winding resistance, and internal deformation removes ambiguity between an interturn defect and a general core or HV-winding displacement.

3.5 Internal Visual Examination and Structural Correlation

Internal examination documented carbon deposits, copper particles, damaged paper insulation, fractured insulating components, and winding deformation concentrated in the LV R-phase region. These observations physically confirm both the location and the high-energy severity of the interturn fault identified electrically.



Figure 10. Internal view of the LV R-phase region showing carbon deposits, copper particles, damaged paper insulation, and winding deformation.

The carbonization and copper particles are direct products of high-temperature arcing and physically validate the D2 diagnosis. The same conductive residue explains the post-event PI and dissipation-factor deterioration, linking the chemical, dielectric, and visual evidence to one arc site.

The fractured spacers and winding deformation demonstrate substantial electrodynamic and thermal stress. Phase-comparative SFRA independently measures the corresponding change in winding electrical characteristics. Together with the repeated through-fault operating history, these findings establish cumulative loss of winding restraint followed by catastrophic deformation and arcing.

4. DISCUSSION: SYNTHESIS OF EVIDENCE AND FAULT PROGRESSION

The synthesis of the comprehensive diagnostic evidence allows for a clear reconstruction of the failure event, an analysis of the protection system's response, and a discussion of the underlying failure mechanism rooted in the long-term aging of the asset.

4.1 Convergent Diagnosis of an Arcing Interturn Fault

The evidence forms a coherent diagnosis of the failure. DGA identifies a D2 high-energy discharge; resistance, ratio, excitation current, dielectric trend, and low-frequency SFRA quantify a marked R-phase anomaly; and internal inspection localizes severe damage to the LV R-phase. This convergence establishes a high-energy arcing interturn fault in that winding.

4.2 Reconstructed Failure Sequence: From Incipient Defect to Catastrophic Breakdown

The reconstructed failure pathway begins with repeated external through-fault exposure, proceeds through cumulative loss of winding restraint and localized insulation integrity, and culminates in the recorded arc. IEC 60076-5 and IEEE C57.109 relate through-fault severity to current magnitude and duration: every operation contributes positive current-squared-time (I^2t) duty, while the associated axial and radial electrodynamic forces scale with current squared [1,16]. The accumulated consequence is measured directly by the R-phase resistance/ratio/excitation asymmetry, low-frequency SFRA interturn signature, fractured spacers, winding deformation, and D2 arcing products.

Stage 1: Operational Stress History

The operating register documents repeated through-fault and in-zone fault protection operations during service. The register records repeated fault operations over the service life: four transformer differential operations associated with reptile (lizard) intrusion in the LV-side kiosk/PT compartments; five LV overcurrent high-set operations with fault current exceeding 4000 A, attributed to cable puncture; and, before revision of the LV high-set setting, three faults cleared by HV overcurrent backup. These operations establish repeated positive I^2t and current-squared electrodynamic duty on the transformer. The measured end-state evidence — R-phase deformation, fractured support components, resistance increase, reduced effective turns, and the configuration-dependent SFRA response — establishes the accumulated mechanical consequence required by the cumulative through-fault-aging mechanism[1,16].

Stage 2: Incipient Insulation Degradation (Years 1–17)

Thermal, moisture, oxygen, and mechanical exposure progressively reduce oil-paper dielectric and mechanical margins. The pre-event GΩ-range megger values show that bulk insulation remained strong while a localized turn-to-turn weak point developed. The later LV-body tan-delta/capacitance shift and carbonized paper demonstrate that this local weakness evolved into the conductive arc path.

Stage 3: Escalation to a Low-Impedance Fault (Pre-Failure)

Repeated mechanical movement, thermal cycling, and electrical stress converted the localized insulation weakness into a low-impedance turn fault. The persistent positive TTR error, ninefold excitation current, and low-frequency SFRA separation demonstrate the reduced-turn loop before the evidence chain culminates in D2 arcing and physical carbonization.

Stage 4: Catastrophic Failure upon Energization

In the failure-event record, the main-tank PRV input asserted at 488.475 ms. RMS values over 50–450 ms were 42.41 A, 36.92 A, and 3.84 A in IA-1, IB-1, and IC-1. The corresponding differential RMS quantities were 0.422 pu, 0.345 pu, and 0.103 pu, with bias quantities of 0.212 pu, 0.173 pu, and 0.052 pu. Current decayed rapidly after the PRV-related digital sequence, establishing the recorded electrical and mechanical protection chronology.

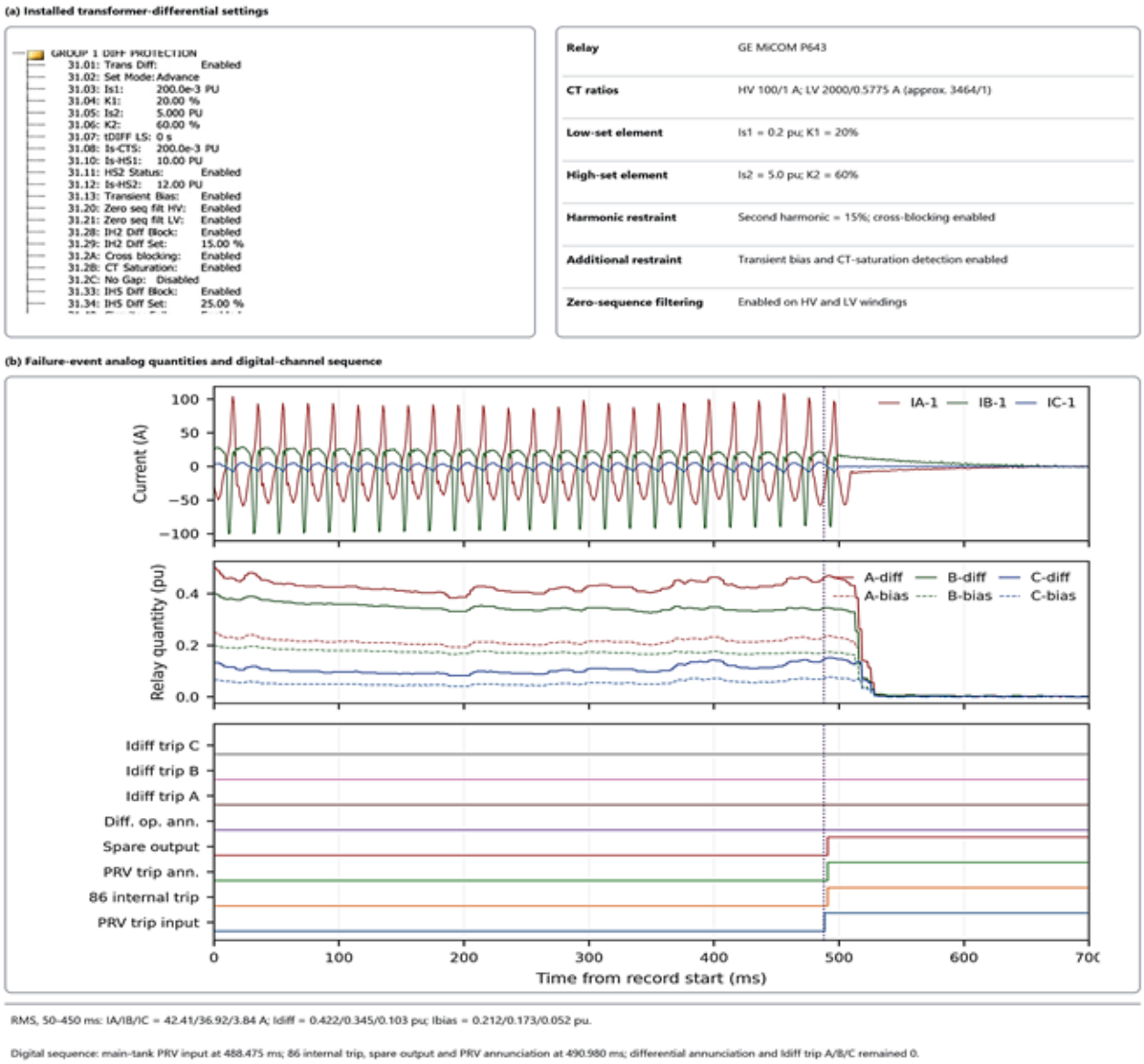


Figure 11. Installed P643 transformer-differential settings and failure-event COMTRADE evidence. The main-tank PRV input asserted at 488.475 ms; the 86 internal-trip, spare-output, and PRV-annunciation channels followed at 490.980 ms, while differential annunciation and Idiff trip A/B/C remained deasserted.

4.3 Analysis of Protection System Response and Implications

The differential RMS quantities were 0.422 pu, 0.345 pu, and 0.103 pu for phases A, B, and C. With Is1 = 0.2 pu and K1 = 20%, the recorded bias remained below the Is1/K1 knee of 1.0 pu. The A- and B-phase operate quantities exceeded the static Is1 level, while transient-bias, second-harmonic, and cross-blocking logic were enabled and the differential annunciation and phase-trip bits remained deasserted. Because the failure occurred during energization, these above-pickup operate quantities coincided with magnetizing inrush, and the enabled second-harmonic and transient-bias stabilization restrained the element so that no trip was issued. At this final event the differential non-

operation reflects inrush stabilization rather than the sub-threshold autotransformer condition described in the Introduction, which governed the earlier incipient stage when the reflected differential current remained below Is1. The event record therefore establishes a restrained 87T response and a successful PRV-initiated mechanical trip sequence[7,17,18].

4.3.1 Differential Protection Non-Operation

Figure 11 presents the installed P643 settings beside the failure-event analog and digital channels. The record demonstrates that the PRV input and 86/annunciation sequence completed while 87T annunciation and all three phase-trip bits remained low. This directly identifies mechanical pressure protection as the operating trip path for the arcing interturn fault.

The PRV supplied the decisive mechanical trip input during the failure. Its operation was complementary to electrical protection: it responded to the internal pressure consequence of the arc while the differential trip outputs remained deasserted.

5. CONCLUSION

The forensic investigation establishes a high-energy arcing interturn fault localized to the LV R-phase winding. Duval geometry, two ratio classifications, and key-gas analysis identify D2, and the APTRANSCO machine-learning ensemble independently corroborates the classification with an assigned 87% probability. R-phase resistance was 19.91% above the Y/B mean, turns-ratio error remained +1.54% to +2.64% across all 17 taps, and excitation current was 9.30 times the Y/B mean. The low-frequency SFRA separation appeared with the LV active and collapsed when it was shorted, establishing the LV R-phase interturn location. Internal carbonization, copper particles, damaged paper, fractured components, and deformation physically validate the diagnosis.

Four differential operations attributed to reptile intrusion, five LV overcurrent high-set operations at fault currents exceeding 4000 A from cable puncture, and three faults cleared by HV overcurrent before the LV high-set revision establish repeated high-current fault exposure over the service life. Representative pre-failure IR values remained in the GΩ range, demonstrating why conventional bulk-insulation checks did not reveal the localized turn weakness. The operating history and the directly measured R-phase mechanical/electrical end state establish a clear causal chain: recurrent reptile-intrusion and cable-puncture faults on the LV side imposed repeated through-fault duty that progressively reduced winding restraint and prepared the LV R-phase interturn breakdown.

The case demonstrates that chemical, electrical, dielectric, frequency-response, relay-setting/event, and physical evidence must be read as a single forensic chain. For comparable assets, retaining disturbance records after every through-fault, preserving baseline SFRA, and trending DGA, IR/PI, tan delta, capacitance, DP, and furan results would convert cumulative-stress assessment from reconstruction to quantified life management. Because mechanical pressure protection — not the differential element — cleared this fault, protection practice for comparable units also warrants review: the second-harmonic and transient-bias inrush-stabilization settings should be checked to avoid over-restraint during energization, and supplementary turn- and earth-fault-sensitive protection (restricted earth fault or negative-sequence supervision), alongside maintained Buchholz and PRV protection, should be considered for incipient interturn faults that terminal-current differential protection cannot detect. The installed unrestrained high-set differential element is set to 12 pu — of necessity, to ride through magnetizing inrush and external through-faults — whereas the fault produced a peak differential of only about 0.42 pu, nearly thirty times below the high-set threshold, so it too could not respond to the interturn fault.

6. REFERENCES

1. International Electrotechnical Commission. IEC 60076-5:2006. Power transformers - Part 5: Ability to withstand short circuit. Geneva: IEC; 2006.
2. Jin M, Chen W, Xu W, Li J, Zhao Y, Zhang Q, Wen T. A path of power transformers failure under multiple short-circuit impacts. Electr Power Syst Res. 2024; 229:110216. https://doi.org/10.1016/j.epsr.2024.110216
3. International Electrotechnical Commission. IEC 60214-1:2014. Tap-changers - Part 1: Performance requirements and test methods. Geneva: IEC; 2014.
4. GE Vernova. MiCOM P40 Agile P64 Transformer Protection Technical Manual. Document No. P64-TM-EN-1-GEV. Paris: GE Vernova; 2025.
5. International Electrotechnical Commission. IEC 60599:2022. Mineral oil-filled electrical equipment in service - Guidance on the interpretation of dissolved and free gases analysis. Geneva: IEC; 2022.
6. IEEE Power & Energy Society. IEEE Std C57.104-2019. IEEE Guide for the Interpretation of Gases Generated in Mineral Oil-Immersed Transformers. New York: IEEE; 2019.
7. International Electrotechnical Commission. IEC 60567:2023. Oil-filled electrical equipment - Sampling of free gases and analysis of free and dissolved gases in mineral oils and other insulating liquids - Guidance. Geneva: IEC; 2023.
8. International Electrotechnical Commission. IEC 60475:2022. Method of sampling insulating liquids. Geneva: IEC; 2022.
9. Reddy RSCV. An integrated, multi-method software platform for advanced dissolved gas analysis in power transformers. Int J Innov Res Technol. 2025; 12(3):2386-2394.
10. Duval M. A review of faults detectable by gas-in-oil analysis in transformers. IEEE Electr Insul Mag. 2002; 18(3):8-17. https://doi.org/10.1109/MEI.2002.1014963
11. IEEE Power & Energy Society. IEEE Std C57.12.90-2021. IEEE Standard Test Code for Liquid-Immersed Distribution, Power, and Regulating Transformers. New York: IEEE; 2021.
12. IEEE Power & Energy Society. IEEE Std C57.152-2025. IEEE Guide for Diagnostic Field Testing of Liquid-Filled Power Transformers, Regulators, and Reactors. New York: IEEE; 2025.
13. International Electrotechnical Commission. IEC 60076-18:2012. Power transformers - Part 18: Measurement of frequency response. Geneva: IEC; 2012.
14. IEEE Power & Energy Society. IEEE Std C57.149-2024. IEEE Guide for the Application and Interpretation of Frequency Response Analysis for Oil-Immersed Transformers. New York: IEEE; 2024.
15. Ni J, Zhao Z, Tan S, Chen Y, Yao C, Tang C. The actual measurement and analysis of transformer winding deformation fault degrees by FRA using mathematical indicators. Electr Power Syst Res. 2020; 184:106324. https://doi.org/10.1016/j.epsr.2020.106324
16. IEEE Power & Energy Society. IEEE Std C57.109-2018. IEEE Guide for Liquid-Immersed Transformers Through-Fault-Current Duration. New York: IEEE; 2018.
17. Venikar PA, Ballal MS, Umre BS, Suryawanshi HM. Sensitive incipient inter-turn fault detection algorithm for power transformers. IET Electr Power Appl. 2016; 10(9):858-868. https://doi.org/10.1049/iet-epa.2016.0059
18. Magrin F. Increasing sensitivity for transformer protection using incremental differential. J Eng. 2018; 2018(15):1209-1215. https://doi.org/10.1049/joe.2018.0262

AUTHOR CONTRIBUTION

R.S. Chanakya Vardhan Reddy conducted the post-failure transformer testing, compiled the failure reports and disturbance records (DR) for analysis, evaluated the data using multiple methodologies, and drafted the original manuscript. H. Ganganna participated in the transformer testing procedures and reviewed the manuscript. B. Venu Madhav reviewed the diagnostic test reports and the final manuscript draft.